

Three-dimensional examination of tearing fracture mechanism of PVC foams via peridynamics

Daud Ali Abdoh¹

Received: 23 December 2024 / Revised: 23 December 2024 / Accepted: 2 May 2025 © The Author(s) 2025

Abstract

Polyvinyl chloride (PVC) foams are primarily used in many industries, such as construction, aerospace, marine, and automotive; thus, understanding their fracture behavior is vital. The paper presents a new study about the three-dimensional fracture behavior of PVC foams using the peridynamic method, where we pay more attention to the tearing fracture mechanics of these foams. We introduce an all-inclusive simulation framework incorporating peridynamic theory to estimate crack propagation in PVC foams. The fracture initiation, growth, and coalescence processes are efficiently captured using the proposed three-dimensional peridynamic model (3D-PDM). The effectiveness and validity of the proposed 3D-PDM are demonstrated through detailed comparisons with experimental data and measurements in predicting fracture patterns and failure loads. The results emphasize the capability of the peridynamic approach in capturing complex fracture phenomena in PVC foams. Therefore, the study provides an efficient tool for researchers and engineers to improve the design of foam-based structures, accordingly enhancing their safety and reliability. Our study not only provides a detailed investigation of the tearing mechanism in PVC foams under various loading and boundary conditions but also highlights the potential of the peridynamic model. The study reveals that bending on PVC foam increases in-plane tearing while decreasing through-the-thickness tearing. Further exploration of the proposed 3D-PDM applications in other polymeric and composite materials could be achieved, offering hope for its potential in fracture mechanics research.

Keywords PVC foam · Failure · Peridynamics · Tearing fracture · Three-dimensional simulation

1 Introduction

Polyvinyl chloride (PVC) foam has gained significant attention across many industries since it is a versatile and lightweight material. The PVC foam is an attractive choice for applications in construction, automotive, aerospace, and marine sectors due to its excellent mechanical properties, thermal insulation, and chemical resistance. A comprehensive understanding of the fracture behavior of PVC foams is crucial for industries such as construction [1, 2], automotive [3, 4], aerospace [5, 6], and marine sectors [7–9]. This understanding can optimize their design and enhance their durability, making PVC foam a more attractive choice for various applications.

☑ Daud Ali Abdoh daud-ali-ahmad.abdoh@polyu.edu.hk; dabdoh2-c@my.cityu.edu.hk

Published online: 05 June 2025

Experiments have been used to investigate the fracture behavior of PVC foams. For example, Aliha and Imani studied the crack initiation angles and propagation paths in PVC foams under mixed modes I/II and I/III loading conditions [10, 11]. Additionally, single-edge notched bending and tensile tests were conducted to assess the impact of defect size on the overall fracture behavior of PVC foams [12]. Furthermore, the fracture and deformation responses of PVC foams have been studied under various loading conditions, such as tension [13], compression [14], shear [15], flexure [16], air blast loads [17, 18], underwater explosions [19], and fatigue [20]. However, experiments may struggle to examine the complex geometries and multiaxial stresses that are found in real-world applications. Moreover, accurate modeling of fracture behavior under localized stress concentrations is challenging. Furthermore, precisely measuring crack initiation and propagation is difficult, as PVC foams are often subjected to complex loading conditions in practical applications, such as bending, compression, and shear. Experimental studies can also be resource-intensive, both in terms of time



Department of Building Environment and Energy Engineering, The Hong Kong Polytechnic University, Kowloon, Hong Kong, China

and cost, with many tests being destructive, thus limiting long-term study capabilities. It is also important to point out that the analysis and interpretation of fracture processes are difficult, and there are higher chances of uncertainty when one translates experimental results into real-world applications. Hence, numerical studies and theoretical models aid a better understanding of the fracture behavior of PVC foams.

Numerical methods have emerged as a robust tool in studying PVC foam fracture behavior, and they offer valuable insights for optimizing PVC foam structural applications. These methods, notably finite element analysis (FEA), enable a detailed crack initiation and propagation simulation under diverse loading conditions [21, 22]. Because of advanced computational models, researchers can effectively mimic the mechanical response of PVC foams. Several numerical methods, such as the extended finite element method (XFEM) [23, 24] and cohesive zone modeling (CZM) [25, 26], are frequently used to simulate crack growth with high fidelity. These approaches, particularly CZM, help describe the fracture toughness and energy absorption capabilities of PVC foams, which are essential for aerospace, automotive, and civil engineering applications. In addition, numerical approaches can examine the effect of microstructure on fracture behavior, which helps design foams with specific attributes. However, the use of mesh-based methods has limitations that can impact the accuracy and efficiency of the simulations. One significant limitation is capturing the complex crack propagation paths and interactions in foam structures. Traditional FEA often necessitates a very fine mesh to accurately model the discontinuities at the crack tip, leading to increased computational costs and time [27, 28]. Additionally, regular re-meshing is required to solve the excessive mesh deformation when the cracks propagate. Therefore, the simulation process becomes more complex, which introduces chances of numerical inaccuracies [29, 30].

The peridynamic method [31, 32] is a meshfree numerical method that has been recently widely used to study the fracture behavior of different materials such as glass [33, 34], steel [35, 36], aluminum [37, 38], and concrete [39–41] since it overcomes the limitations associated with traditional meshbased methods. For instance, the peridynamic method does not require a predefined mesh, which allows for mesh-free simulation of crack initiation and propagation [42, 43]. Additionally, a more accurate representation of fracture processes is feasible by the peridynamic approach since it naturally handles discontinuities and large deformations [44, 45]. The nonlocal nature of the peridynamic method and its usage for integral equations rather than differential equations facilitate examining the actual fracture mechanics of the foam materials through the simulation of long-range forces and interactions. The capability of the peridynamic approach of simulating crack formations, as well as their interactivity with the internal structure of foam without incurring too much processing power, becomes a significant asset in the enhancement and utilization of PVC foams in industries that call for high-strength and durable but lightweight materials.

Peridynamics lends itself well to simulating the dynamic evolution of tearing fractures in PVC foams, which is important for examining the distinctive tearing characteristics of such materials. Knowing how PVC foams respond to tearing forces enables engineers to design safer and more durable products, particularly in applications where failure could pose significant safety hazards, such as in aircraft or building structures. In addition, understanding the behavior of tearing fractures enables improvements to the material characteristics of PVC foams by increasing their overall strength and toughness and their resistance to crack propagation and by creating new formulations or composites with superior properties. Moreover, manufacturers can develop PVC foams with higher performance of efficiency and economic viability.

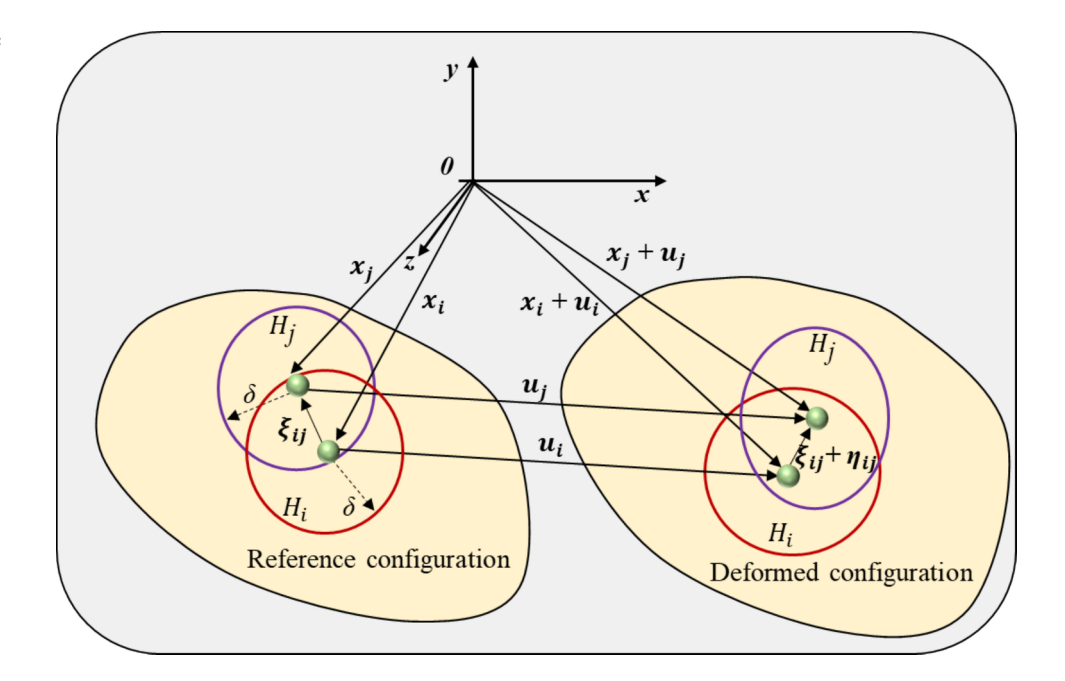
This research paper marks a significant breakthrough in the scope of fracture mechanics of PVC foams as it investigates, for the first time, the three-dimensional tearing fracture behavior of the material. The results obtained in this study are relevant in practice. We start by using experiments to validate the proposed three-dimensional peridynamic model (3D-PDM) under various loading and boundary conditions. Once the 3D-PDM is validated, we investigate the tearing response of PVC foam under different conditions and propose essential concluding remarks about the tearing strength of PVC foams. We outline the remainder of this paper as follows: Sect. 2 details the modeling techniques used in the 3D-PDM. Section 3 describes the comprehensive validation process, where the 3D-PDM is rigorously validated against experimental measurements and observations. We also explore the fracture behavior of PVC foams under tearing loads in different directions and various confined conditions. Finally, we present the conclusions in Sect. 4.

2 Numerical modeling

In peridynamics, each particle interacts with other particles within a specific horizon (H) and a predefined distance (δ) . This nonlocal interaction contrasts with classical mechanics, where interactions are typically considered local. The nonlocal nature of peridynamics is a fundamental feature that sets it apart from classical continuum mechanics and offers significant advantages for modeling long-range forces and simulating phenomena such as crack propagation. Figure 1 shows the peridynamic variables adopted to model the bond deformation between two particles, i and j. On the one hand, ξ_{ij} is the initial relative distance between two particles i and j in the undeformed (reference) configuration as given in Eq. (1) [33, 38, 43]. On the other hand, η_{ij} is the change in



Fig. 1 Details of the peridynamic terminology used to describe the bond deformation between two particles



distance between the particles i and j after the deformation as given in Eq. (2) [33, 38, 43]. The radius or the size of particle interaction is controlled by the horizon radius (H_i) .

$$\xi_{ii} = x_i - x_j, \tag{1}$$

$$\eta_{ij} = u_i - u_j, \tag{2}$$

Equation (3) [33, 38, 43] is the integral equation of peridynamics that relates the force density of the particle i to the relative positions of neighboring particles j, where b, ρ_i and a_i are the external force, density, and acceleration of particle i, respectively. The peridynamic force between particles i and j, as shown in Eq. (4) [33, 38, 43], relays on the bond's stiffness (c) and the bond's elongation ratio (s_{ij}) . The calculation of the bond's stiffness (c) and the bond's elongation ratio between particles i and j (s_{ij}) are depicted in Eqs. (5) and (6) [33, 38, 43], respectively. The bond's critical stretch (s_0) presents the maximum elongation that the peridynamic bond can take before breakage, as shown in Eq. (7) [33, 38, 43], where E is Young's modulus and σ_{max} is the maximum fracture strength. Therefore, when the variable μ = 0, the peridynamic bond is broken and vice versa, as shown in Eq. (8) [33, 38, 43].

$$\rho_i \mathbf{a}_i = \int f(\boldsymbol{\xi}_{ij}, \, \boldsymbol{\eta}_{ij}) dV + \mathbf{b}, \tag{3}$$

$$f(\eta_{ij}, \xi_{ij}) = \begin{cases} \frac{\xi_{ij} + \eta_{ij}}{\|\xi_{ij} + \eta_{ij}\|} \mu c s_{ij}, & \xi \leq \delta \\ 0, & \xi > \delta \end{cases}$$
(4)

$$c = \frac{12E}{\pi \delta^4},\tag{5}$$

$$s_{ij} = \frac{||\eta_{ij} + \xi_{ij}|| - ||\xi_{ij}||}{||\xi_{ij}||},\tag{6}$$

$$s_o = \frac{\sigma_{max}}{E},\tag{7}$$

$$\mu = \begin{cases} 1, \ s_o < s_{ij} \\ 0, \ s_o \ge s_{ij} \end{cases},\tag{8}$$

Equations (9), (10), and (11) [38] show the calculation of forces acted on each particle (i) at the time (t) in the x-, y-, and z-directions, respectively. It is worth noting that Eqs. (9), (10), and (11) are like Eq. (3) but with considering the effects of all nearby particles (j), which N_{Hi} represents the total number of nearby particles (j) around the main particle (i). Moreover, x_{ij} , y_{ij} and z_{ij} refer to the distances between particles i and j in the x-, y- and z- directions, respectively.

$$F_{xi}(t) = \sum_{j=1}^{N_{Hi}} \frac{x_{ij}}{||\boldsymbol{\xi}_{ij} + \boldsymbol{\eta}_{ij}||} \mu c s_{ij}(t), \tag{9}$$

$$F_{yi}(t) = \sum_{j=1}^{N_{Hi}} \frac{y_{ij}}{||\boldsymbol{\xi}_{ij} + \boldsymbol{\eta}_{ij}||} \mu c s_{ij}(t), \tag{10}$$

$$F_{zi}(t) = \sum_{j=1}^{N_{Hi}} \frac{z_{ij}}{||\boldsymbol{\xi}_{ij} + \boldsymbol{\eta}_{ij}||} \mu c s_{ij}(t), \tag{11}$$

Equations (12), (13), and (14) calculate the acceleration for each particle (i) according to the sum forces acting on it in the x-, y- and z-directions [38], respectively. Therefore, the new velocities are obtained using Eqs. (15), (16), and (17)



[38], respectively, where Δt is the time step.

$$a_{xi}(t) = \frac{F_{xi}(t)}{\rho_i},\tag{12}$$

$$a_{yi}(t) = \frac{F_{yi}(t)}{\rho_i},\tag{13}$$

$$a_{zi}(t) = \frac{F_{zi}(t)}{\rho_i},\tag{14}$$

$$v_{xi}(t) = a_{xi}(t)\Delta t + v_{xi}(t - \Delta t), \tag{15}$$

$$v_{vi}(t) = a_{vi}(t)\Delta t + v_{vi}(t - \Delta t), \tag{16}$$

$$v_{zi}(t) = a_{zi}(t)\Delta t + v_{zi}(t - \Delta t), \tag{17}$$

Displacements for each particle i in the x-, y-, and z-directions $(u_{xi}(t), u_{yi}(t))$ and $u_{zi}(t)$ at time instant t are calculated according to the average velocities in the current and previous time instants $(t \text{ and } t - \Delta t)$, as shown in Eqs. (18), (19), and (20), respectively [38].

$$u_{xi}(t) = 0.5(v_{xi}(t) + v_{xi}(t - \Delta t))\Delta t,$$
 (18)

$$u_{yi}(t) = 0.5 \left(v_{yi}(t) + v_{yi}(t - \Delta t) \right) \Delta t, \tag{19}$$

$$u_{7i}(t) = 0.5(v_{7i}(t) + v_{7i}(t - \Delta t))\Delta t, \tag{20}$$

Peridynamic bonds are broken due to the large displacements and deformations occurring in the solid body. Accordingly, the damage $(D_i(t))$ in each particle i and time instant (t) increases based on the numbers of broken and unbroken bonds, as shown in Eq. (21) [33, 38, 43].

$$D_i(t) = 1 - \frac{\sum_{j=1}^{N_{Hi}} d(\xi_{ij}, \eta_{ij})}{N_{Hi}},$$
(21)

Figure 2 illustrates the procedural steps of the 3D-PDM, a computational framework designed to model fractures and deformations in PVC foams under various loading and boundary conditions. The process begins with defining the geometry and material properties of the PVC foam, along with the coordinates of its particles. Subsequently, bond stiffness (c) and bond's critical stretch (s_o) are calculated using Eqs. (5) and (7), respectively. Initially, dynamic loadings are applied to constrained particles by assigning displacement values (u). As a result, the forces in the peridynamic bonds and the particles' accelerations, velocities, and displacements are computed for each direction (x, y, z). Following this, boundary conditions are enforced, and the particle coordinates are updated. Finally, the damage value $(D_i(t))$ is determined using Eq. (21).



3.1 Validation

First, we validate the proposed 3D-PDM by comparing its fracture simulation results with experimental measurements and observations in two cases. The first case involves a pure mode I test, while the second case involves a mixed-mode I and II test. The validity of the proposed 3D-PDM is confirmed when it is verified in these two different tests under varying loading and boundary conditions.

3.1.1 Pure mode I test

In the pure mode I test, the PVC foam sample is placed on two fixed roller supports, with a distance of 120 mm between them, as shown in Fig. 3. The 20 mm thick PVC foam sample, a half-circle with an 80 mm radius, features a 40 mm long notch at its center. Figure 3 also illustrates the peridynamic discretization of the problem, where enlargement E1 shows the peridynamic interaction between the main particle i and nearby particles j. The particles at the loading location are subjected to a displacement loading in the y-direction (u_y) of -2 mm/min. Additionally, the particles at the fixed roller support experience zero displacements in the y-direction ($u_y = 0$), as depicted in Fig. 3.

The Young's modulus (E), maximum fracture strength (σ_{max}), and density (ρ) of PVC foam are 227 MPa, 5.36 MPa, and 200 kg/m³ [22], respectively. The PVC foam sample consists of 19,176 particles, with a spacing of 1.25 mm in both the x- and y-directions. Three surfaces represent the sample through its thickness. The horizon radius (δ) in the x-y plane is set to 3.75 mm (3 times the particle spacing), and the maximum elongation at fracture (s_o) is determined using Eq. (7). The time step (Δt) is 0.15 μ s. These peridynamic modeling parameters are consistently applied in all simulation cases throughout this paper.

When loading is applied to the top of the PVC foam sample, the top particles move downward at a rate of 2 mm/min. This movement deforms the peridynamic bonds, generating forces in all directions, as described in Sect. 2. Consequently, the particles accelerate and move according to these forces, resulting in displacement. For example, Fig. 4 shows contour plots of displacements in the x and y directions (u_x and u_y) at simulation step number (SSN) equals 500. In the x-direction, the maximum and minimum displacement values are -10.3×10^{-7} m and 10.3×10^{-7} m, respectively, indicating that particles at the right edge move right by 10.3×10^{-7} m, and particles at the left edge move left by 10.3×10^{-7} m. In the y-direction, the maximum and minimum displacement values are -12.9×10^{-7} m and 2.23×10^{-7} m, respectively. Therefore, the particles at the top, where the loading



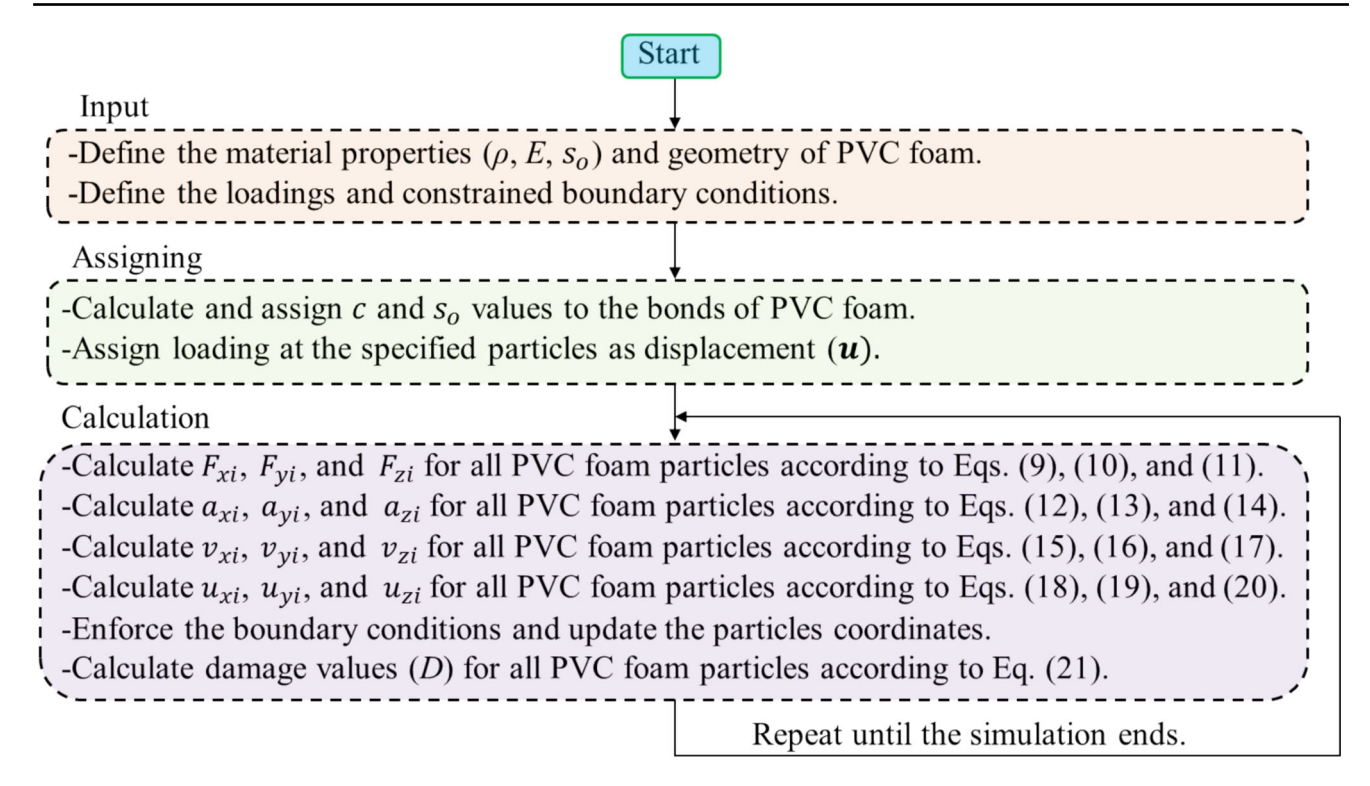


Fig. 2 Summary of procedural steps of the 3D-PDM used to model fractures in PVC foams

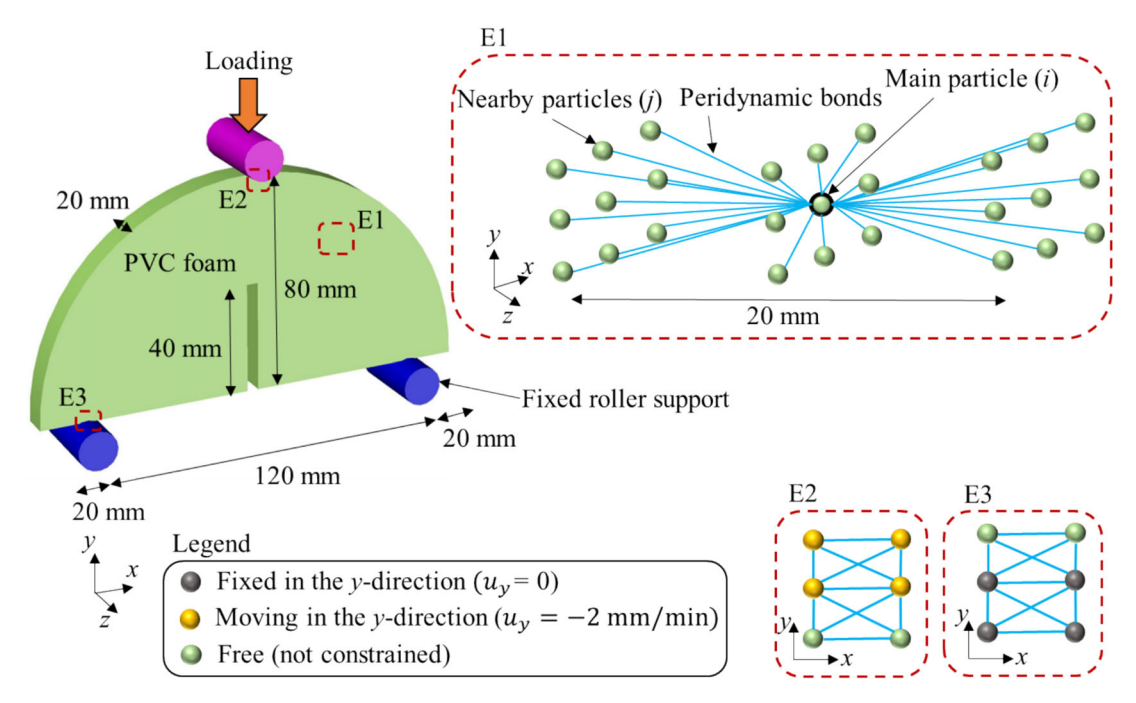
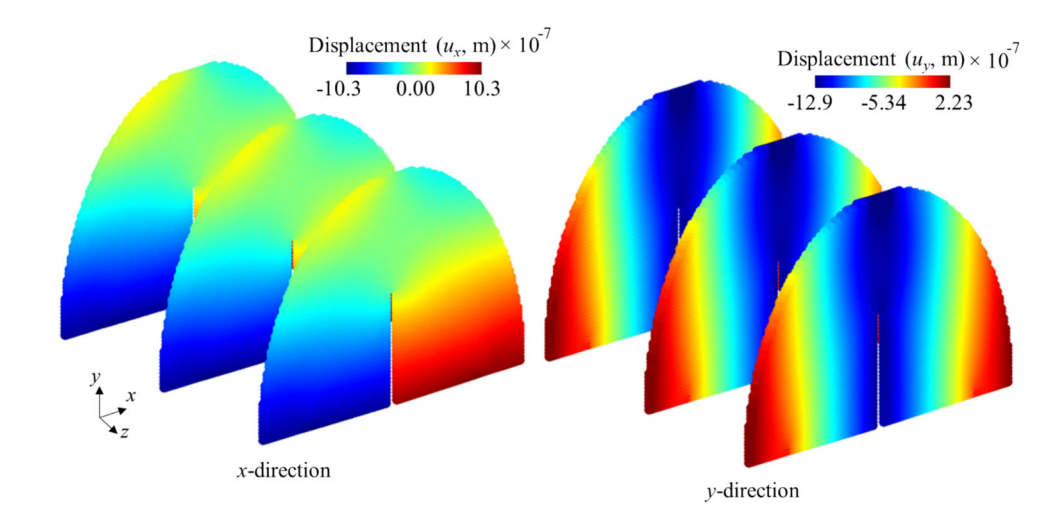


Fig. 3 Problem description and peridynamic discretization of the pure mode I test

Fig. 4 Contour plots of displacements in the x- and y-directions $(u_x \text{ and } u_y)$ at SSN = 500



is applied, experience the highest displacement values ($u_y = -12.9 \times 10^{-7}$ m).

When the elongation of a bond surpasses its critical stretch (s_o) , the bond breaks, leading to an increase in damage, as depicted in Fig. 5(a). It's important to note that fracture initiates from the notch tip due to the highest stress concentration at that point. Subsequently, the fracture propagates upwards until it approaches the region where the load is applied. Figure 5(b) illustrates that the final fracture shapes observed in experimental and 3D-PDM scenarios are similar. Furthermore, the graphs depicting force variation with cumulative displacement in the y-direction (Δ_y) from experiment [22] and 3D-PDM show a good agreement, as illustrated in Fig. 5(c). This substantial agreement between the two methods underscores the reliability and trustworthiness of the 3D-PDM method in predicting the fracture behavior of PVC foam.

3.1.2 Mixed-mode I and II test

To confirm the validity of the 3D-PDM, we use it to simulate fractures in PVC foam under mixed-mode I and II tests. The same configuration and peridynamic discretization from the pure mode I test are applied here but with the left roller support positioned near the center, as shown in Fig. 6. Consequently, the fracture propagates from the notch tip toward the top location at an angle, as illustrated in Fig. 7(a). The final fracture shapes obtained from the experiment and 3D-PDM are similar, as depicted in Fig. 7(b). Additionally, the plots of force variation with cumulative displacement in the y-direction (Δ_y) from experiment [22] and 3D-PDM show good agreement, as presented in Fig. 7(c). Thus, 3D-PDM effectively predicts the fracture behavior of PVC foam under complex loading conditions.



3.2 New cases

In this section, we employ the 3D-PDM to investigate the tearing fracture behavior of PVC foam in the *x*- and *y*-directions for the first time. The same configuration and setup as in the pure mode I test are used, but with additional loads applied at the roller support in the *x*- and *y*-directions to simulate tearing in the PVC foam. These new findings underscore the critical importance of understanding the tearing mechanism in PVC foam to enhance the design quality of these materials.

3.2.1 Tearing fracture behavior in the x-direction

In this section, we analyze the tearing fracture behavior of PVC foam in the x-direction (in-plane tearing) using the validated 3D-PDM model. New loads are applied in the x-direction at both support rollers, as illustrated in Fig. 8. Consequently, the particles at the roller locations experience a loading displacement in the x-direction (u_x) of 20 mm/min, with no loading displacement in the y-direction (u_y). It's important to note that these x-direction loadings are applied after the temporary vertical loading displacement at the top of the PVC foam, as depicted in Fig. 8. Thus, there are two stages of loading: in the first stage, a vertical displacement is applied until the particles at the top move downward by a distance denoted by Δ_y . Following this, a loading displacement in the x-direction (u_x) of 20 mm/min is applied to the particles at the roller supports, as shown in Fig. 8.

First, we investigate the tearing fractures in the x-direction without applying vertical loads ($\Delta_y = 0$ mm), as illustrated in Fig. 9. The force and cumulative displacement in the x-direction are recorded for the particles at the roller supports. The force in the x-direction (F_x) increases to 827 N when the displacement reaches 3.36 mm. Subsequently, as the displacement in the x-direction continues to increase, the force

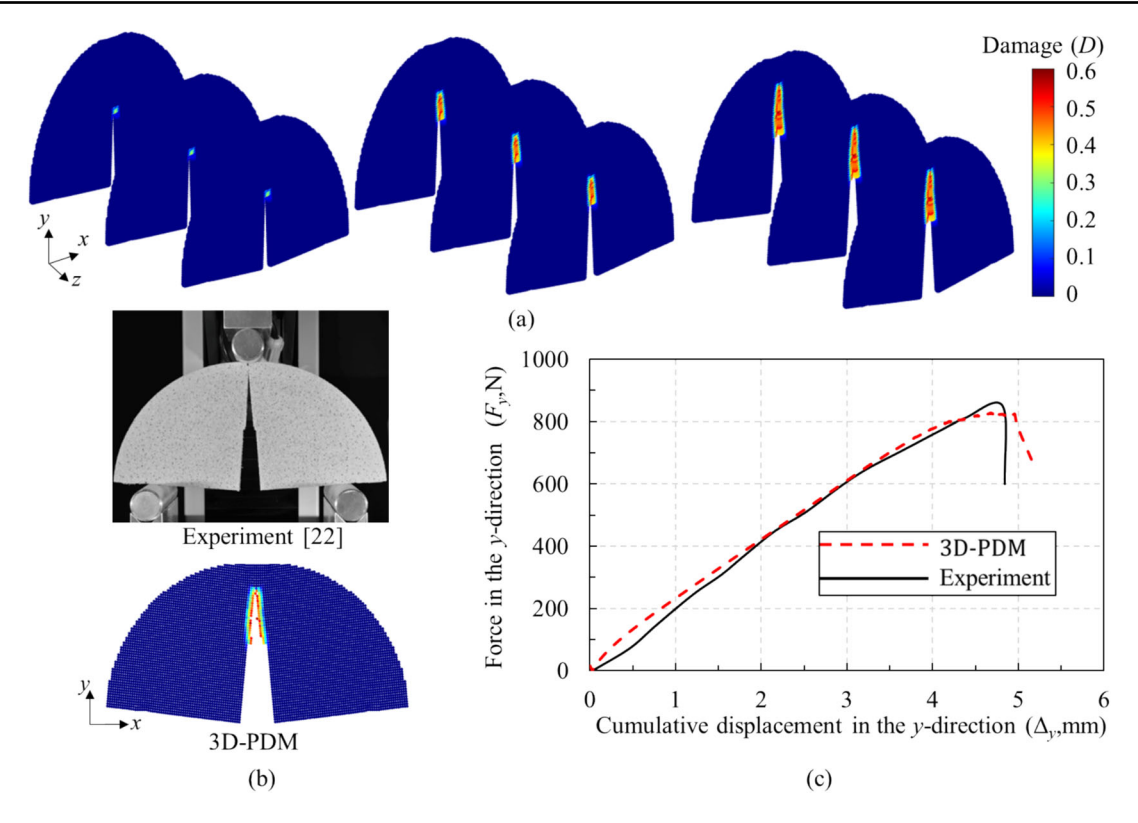


Fig. 5 Fracture results of the pure mode I test: **a** damage contour plots in the PVC foam at different simulation steps using the 3D-PDM; **b** final fracture shapes in the PVC foam obtained from experiment [22] and

3D-PDM; ${\bf c}$ plots of force variation with cumulative displacement in the y-direction (Δ_y) obtained from experiment [22] and 3D-PDM

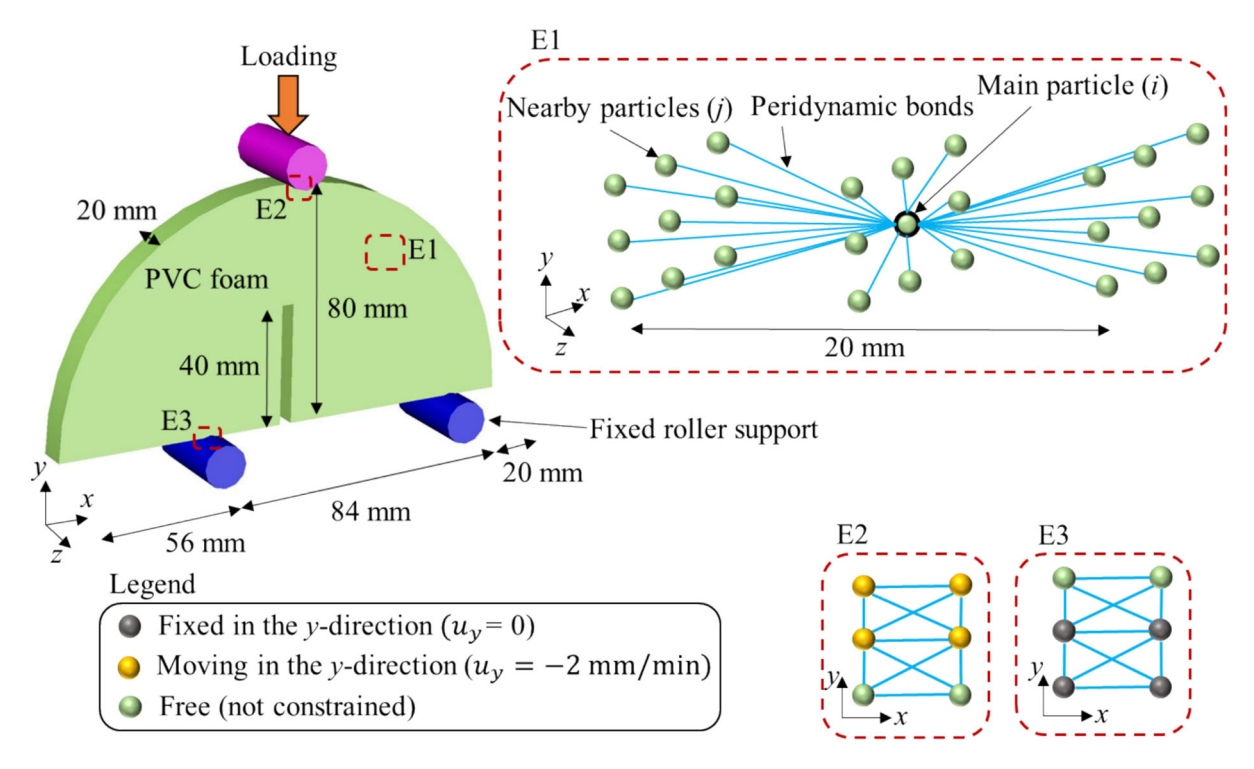


Fig. 6 Problem description and peridynamic discretization of the mixed-mode I and II test

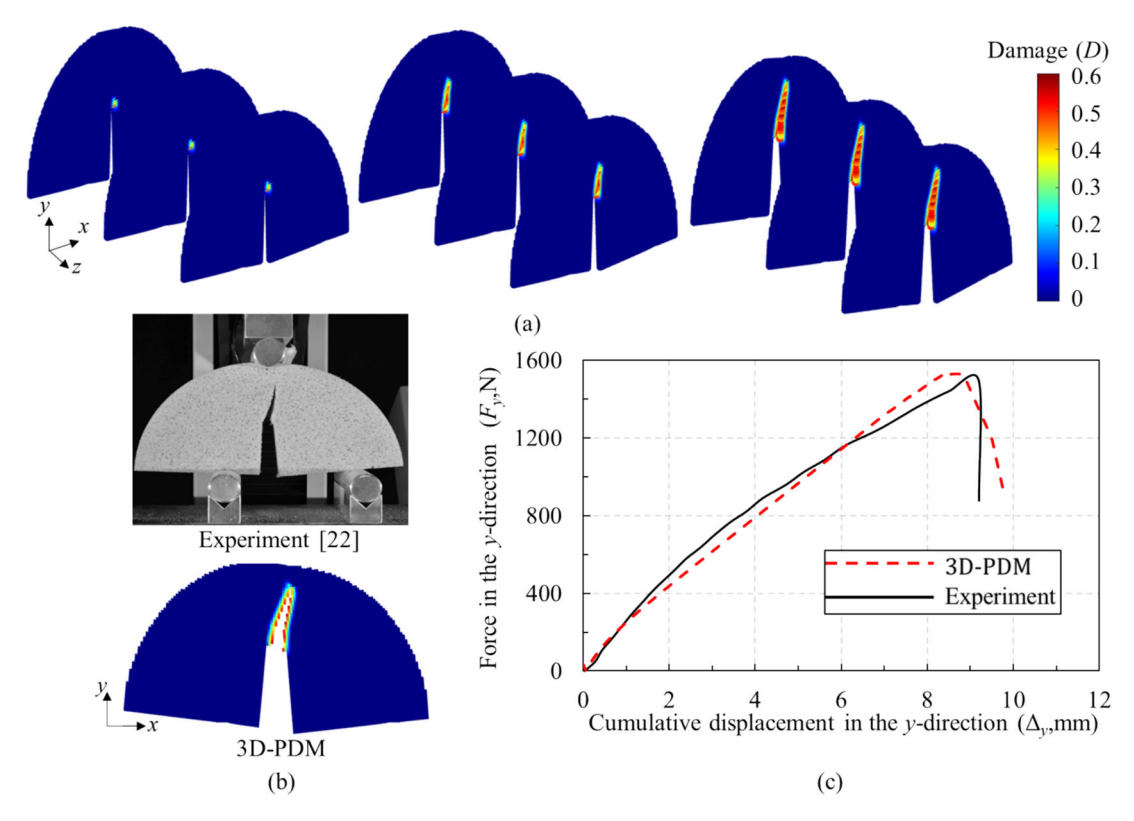


Fig. 7 Fracture results of the mixed-mode I and II test: a damage contour plots in the PVC foam at different simulation steps using the 3D-PDM; b final fracture shapes in the PVC foam obtained from experiment [22]

and 3D-PDM; c plots of force variation with displacement in the y-direction obtained from experiment [22] and 3D-PDM

Table 1 Summary of cumulative displacement and force values in the *x*-direction at different values of Δ_y

Δ_y (mm)	Δ_x (m) due to loading in the y-direction	Total Δ_x (m)	Maximum F_x (N)
0	0.00	3.36	827
1	0.59	3.44	811
2	1.43	3.57	754
3	2.26	4.36	689

decreases, and fractures propagate through the top of the PVC foam sample, as shown in Fig. 9. Thus, failure occurs when the force in the *x*-direction reaches 827 N, marking the initiation of the fracture at that force level.

In Fig. 10, we examine the effects of initially applying vertical loadings (bending actions) followed by loadings in the x-direction. Notably, as the duration of vertical loading at the top of the PVC foam sample increases, tearing fractures occur at lower forces in the x-direction. For example, the maximum forces in the x-direction (F_x) are 827 N, 810 N, 754 N, and 689 N when Δ_y values are 0 mm, 1 mm, 2 mm, and 3 mm, respectively, as shown in Fig. 10 and Table 1. This

indicates that the tearing strength in the x-direction decreases by approximately 17% when the top particles move downward by 3 mm (3.75% of its height) under bending actions. This decrease in tearing capacity suggests that the material's resistance to in-plane tearing is significantly affected by the application of bending loadings. Therefore, bending loadings significantly accelerate tearing in the x-direction (in-plane tearing). Additionally, Δ_x initially increases due to the vertical loading applied at the top of the PVC foam and increases again due to the loading in the x-direction. For instance, Δ_x increases from 0 to 0.59 mm due to vertical loading when $\Delta_v = 1$ mm and then Δ_x increases again from 0.59 to 3.44 mm due to the x-direction loading, as shown in Table 1 and Fig. 10(a). Table 1 also summarizes the values of Δ_x and maximum F_x at different values of Δ_y , highlighting that tearing strength decreases as bending loading increases.

3.2.2 Tearing fracture behavior in the z-direction

This section explores the tearing fracture behavior of PVC foam in the *z*-direction (through-the-thickness tearing) using the 3D-PDM. In this context, new loadings are introduced in the *z*-direction at both support rollers, as shown in Fig. 11. The particles at the roller locations consequently undergo a



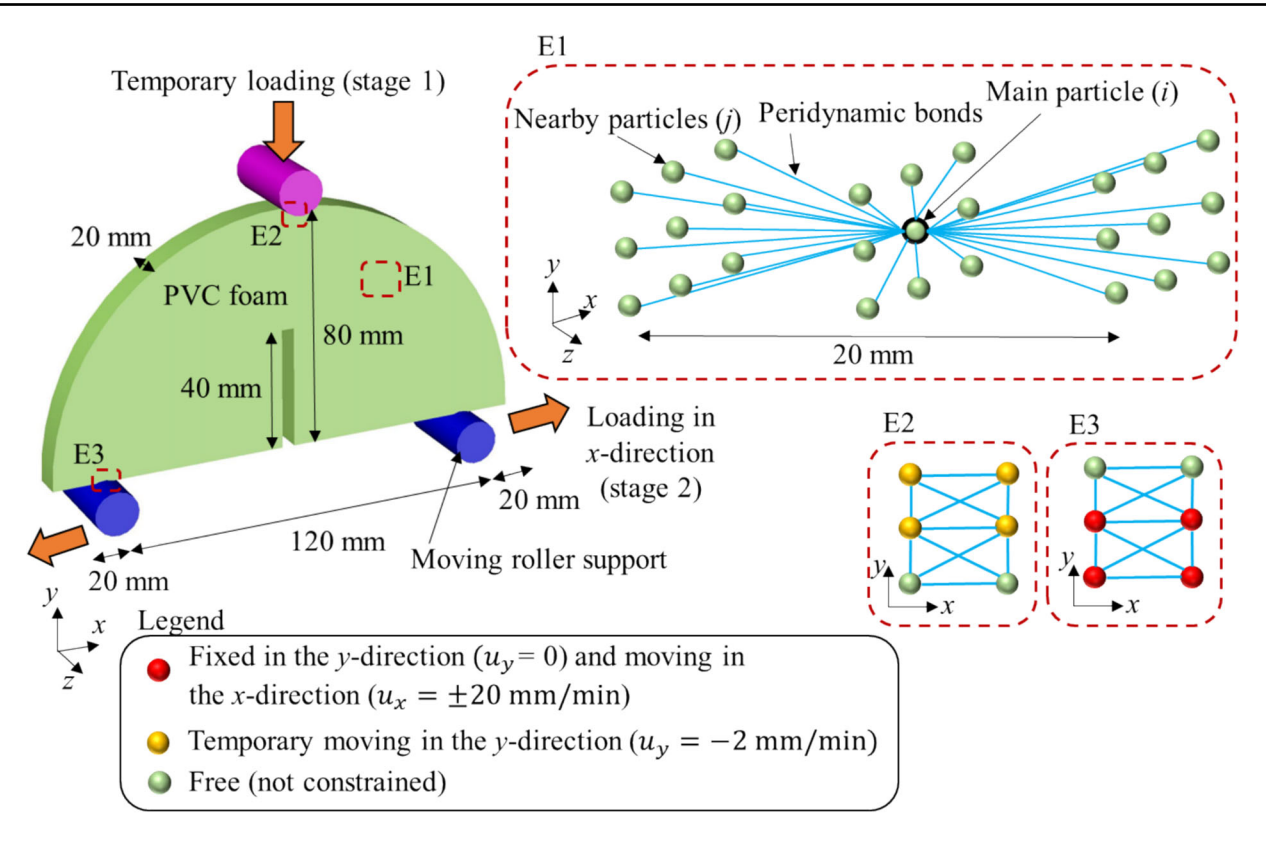
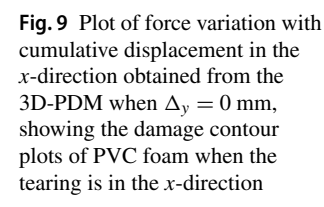
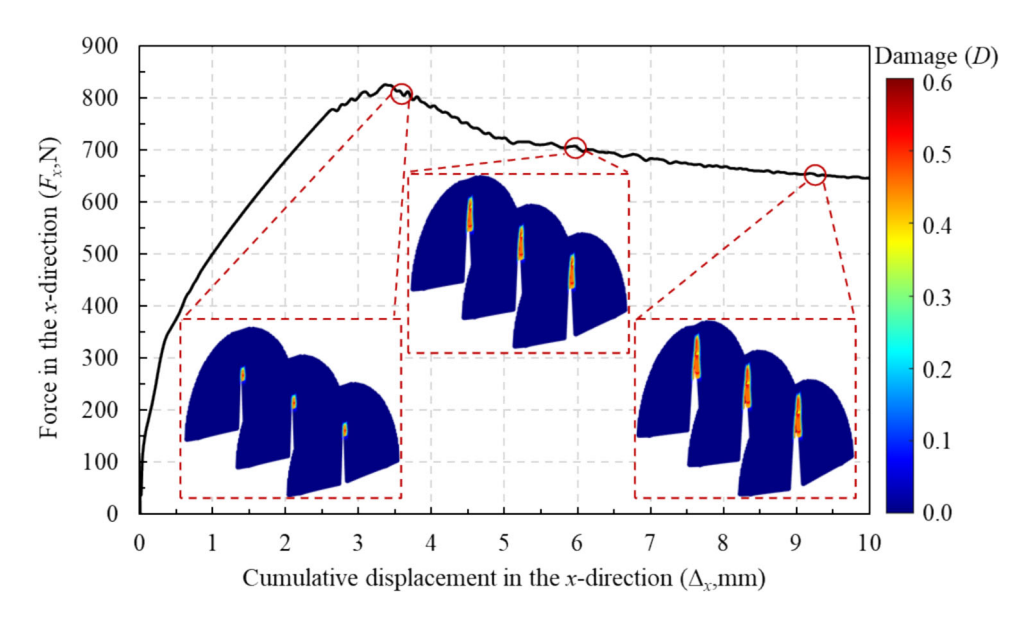


Fig. 8 Problem description and peridynamic discretization of the tearing fracture in the x-direction (in-plane tearing)





loading displacement in the z-direction (u_z) of 20 mm/min, with zero loading displacement in the y-direction (u_y) . It's important to note that the loadings in the z-direction are applied after the temporary loading at the top of the PVC foam, as shown in Fig. 11. This results in a two-stage loading process: the first stage involves applying vertical displacement until the particles at the top move downward by a

distance Δ_y . Subsequently, a loading displacement in the z-direction (u_z) of 20 mm/min is applied to the particles at the roller supports, as depicted in Fig. 11.

First, we investigate the tearing fractures in the z-direction (through-the-thickness tearing) without applying vertical loadings ($\Delta_y = 0$ mm), as shown in Fig. 12. The force and cumulative displacement in the z-direction are recorded for the particles at the roller supports. The force in the z-direction



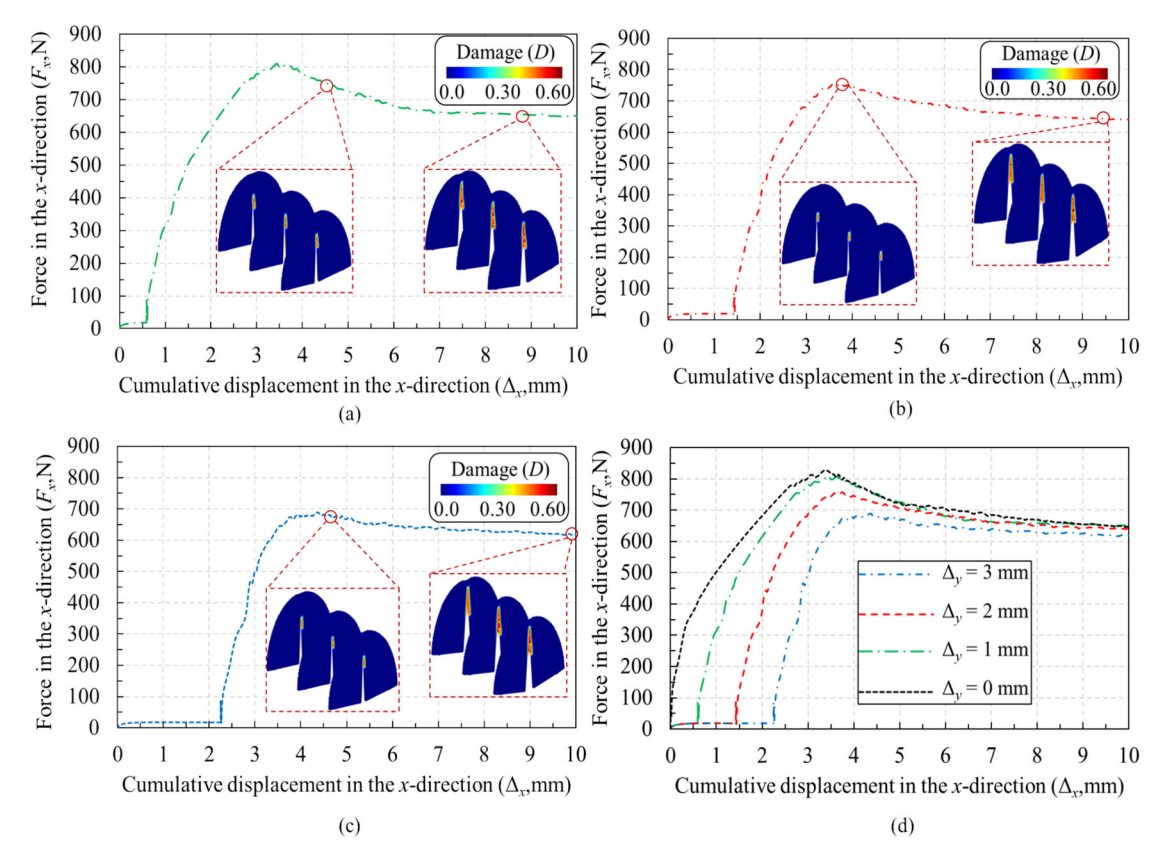


Fig. 10 Plot of force variation with displacement in the *x*-direction obtained from the 3D-PDM showing the damage contour plots of PVC foam when the tearing is in the *x*-direction: **a** at $\Delta_y = 1$ mm; **b** At Δ_y

= 2 mm; ${\bf c}$ At Δ_y = 3 mm; ${\bf d}$ comparison between force variation with cumulative displacement plots at different values of Δ_y

increases to 847 N when the displacement in the z-direction reaches 82 mm. Beyond this point, the force decreases as the cumulative displacement continues to increase, and the fracture propagates through the top of the PVC foam sample, as depicted in Fig. 12. Additionally, we define three main zones for the through-the-thickness tearing process: (1) the no crack zone when Δ_z ranges from 0 to 40 mm, (2) the crack propagation zone when Δ_z ranges from 40 to 82 mm, and (3) the complete separation zone when Δ_z exceeds 82 mm.

In Fig. 13, we examine the effects of applying vertical loadings before the loadings in the z-direction. We highlight an additional zone, the safety zone, where Δ_z ranges from 0 to 20 mm, indicating that the PVC foam material is far from fracture. As the duration of vertical loading application at the top of the PVC foam sample increases, tearing fractures occur at higher loadings in the z-direction at $\Delta_z = 20$ mm (the end of the safety zone). For example, the maximum forces in the z-direction are 474 N, 489 N, 508 N, and 528 N when Δ_y is 0 mm, 1 mm, 2 mm, and 3 mm, respectively, as shown in Fig. 13 at $\Delta_z = 20$ mm. Thus, we conclude that tearing strength in the z-direction increases by approximately 11% when the top particles move downward by 3 mm (3.75% of its

height) under bending actions. Therefore, the bending load decelerates tearing in the *z*-direction (through-the-thickness tearing), a finding that has practical implications for material design and engineering.

Our exploration into how confining the PVC foam in the z-direction affects the tearing fracture behavior in the same direction has led to interesting findings. In this scenario, we do not apply vertical loading. Instead, we constrain all PVC foam particles from moving in the x-direction by applying zero displacement values in that direction ($u_x = 0$) to simulate the confining condition. It's important to note that confining does not compress the PVC foam but prevents it from moving in the x-direction. Our analysis, depicted in Figs. 14 and 15, reveals that confining the PVC foam in the x-direction decreases its tearing strength in the z-direction (through-thethickness tearing). For instance, the maximum force in the z-direction (F_z) decreases from 847 to 806 N, as shown in Fig. 14. Additionally, we observe that fracture propagation is faster in the confined case, as shown in Fig. 15 at $\Delta_7 = 60$ mm. This physical phenomenon can be explained using the 3D-PDM as follows: in the confined case, where particles are not allowed to move in the x-direction, movement and fracture



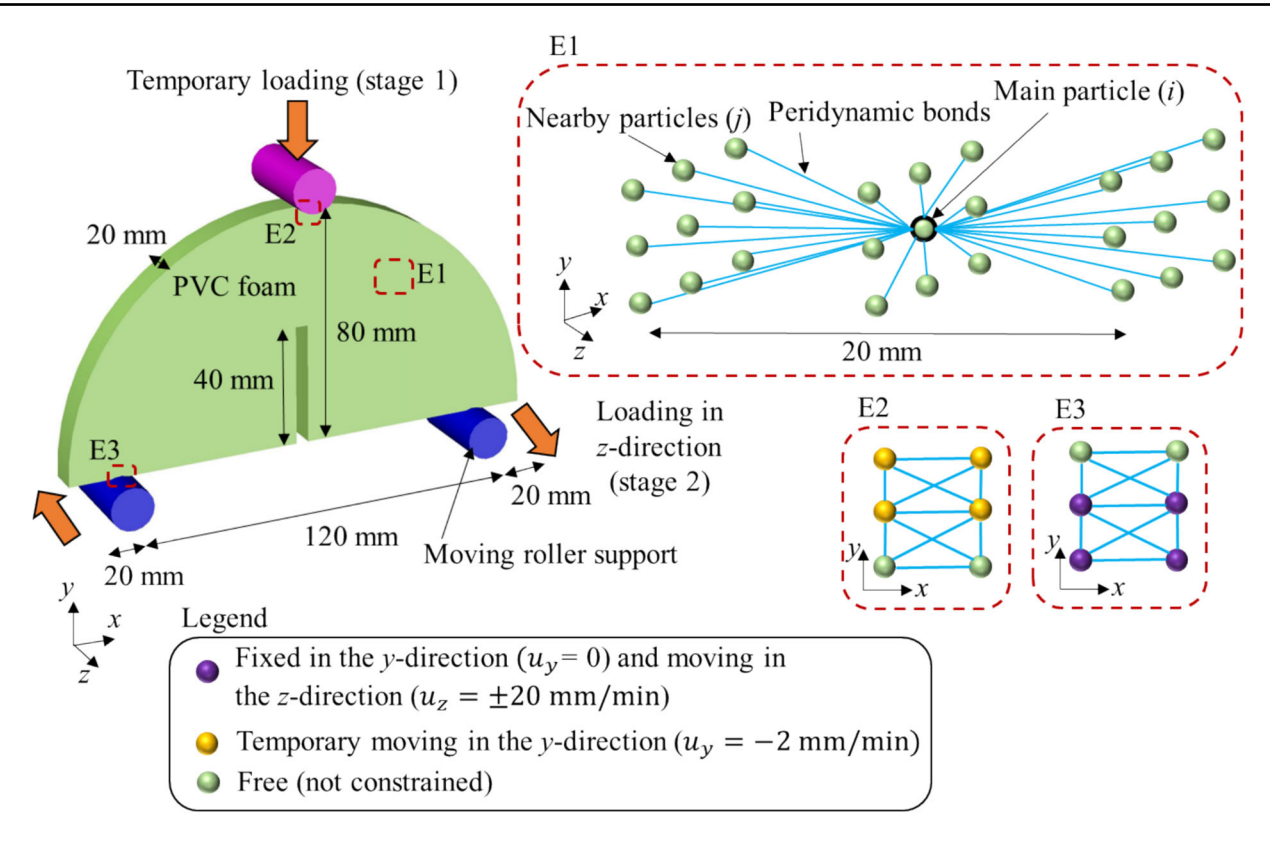
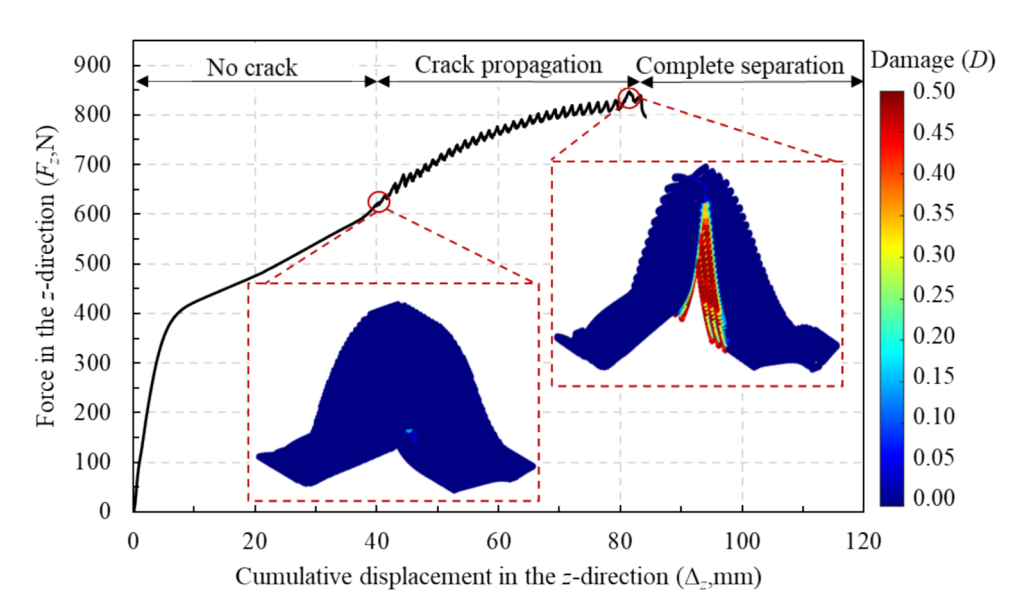


Fig. 11 Problem description and peridynamic discretization of the tearing fracture in the z-direction (through-the-thickness tearing)

Fig. 12 Plot of force variation with displacement in the z-direction obtained from the 3D-PDM when $\Delta_y=0$ mm, showing the damage contour plots of PVC foam when the tearing in the z-direction



are concentrated solely in the z-direction. Consequently, the peridynamic bonds are deformed only in the loading direction (z-direction), leading to increased bond breakage and damage in the confined case.

4 Conclusions

The findings of this research contribute significantly to the understanding of fracture mechanics in PVC foams, which is essential in aerospace, marine, automotive, and construction applications. The peridynamic method has been used to model the three-dimensional fracture of PVC foams, emphasizing tearing types of fractures. The established simulation



Fig. 13 Plots of force variation with displacement in the *z*-direction at different values of cumulative vertical displacement (Δ_v)

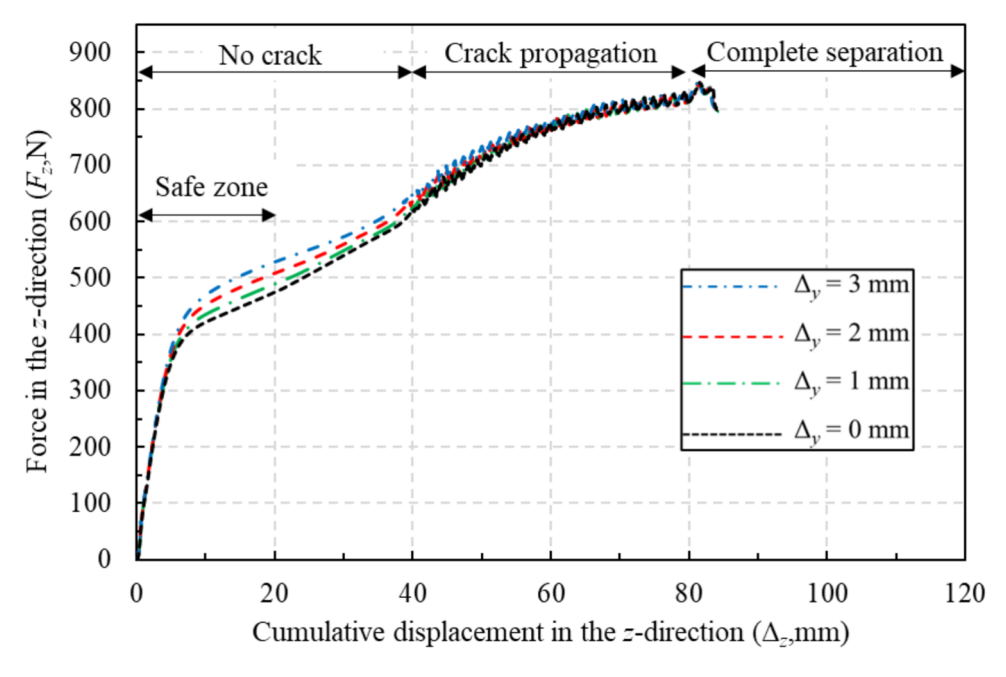
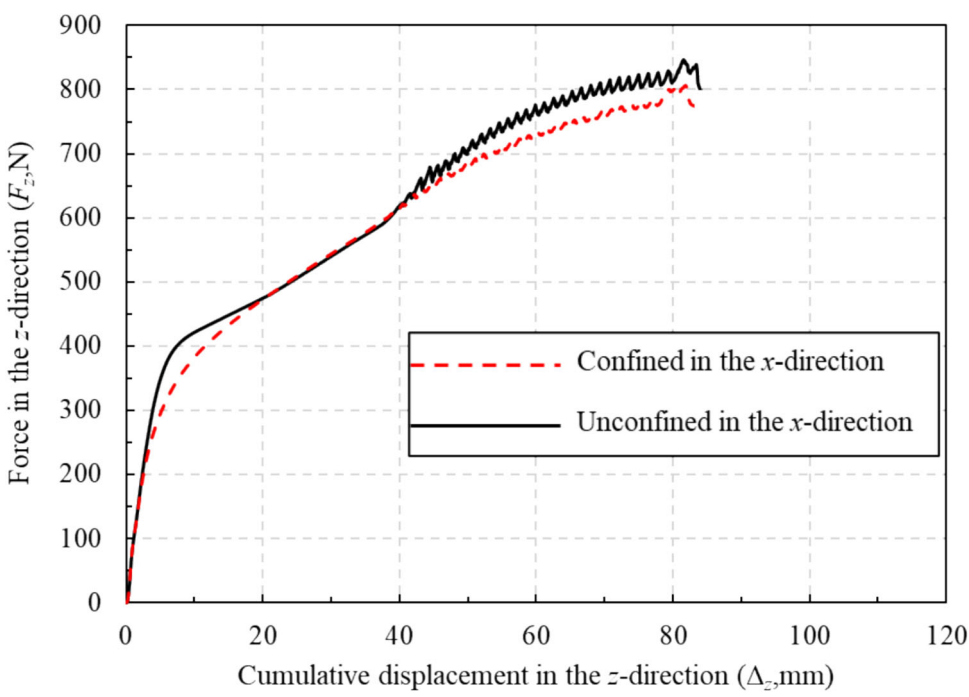


Fig. 14 Plots of force variation with cumulative displacement in the *z*-direction in the confined and unconfined cases in the *x*-direction



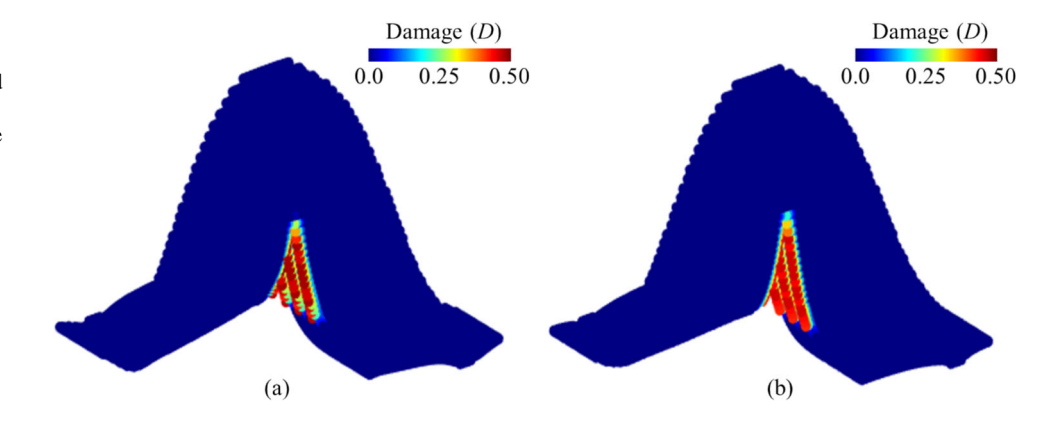
framework, which is based on the peridynamic theory, has shown the ability to model initiation, propagation, and interaction of cracks subjected to different loading conditions. Thus providing insight into the failure and fracturing processes in PVC foams. Through validation processes, it has been established that the peridynamic model performs adequately with respect to the prediction of fracture patterns as well as failure loads when correlated with experimental data. Consequently, this validation offers some validation of the ability of the peridynamic approach to predict intricate

fracture patterns of PVC foams and to have better material development, as well as help guarantee the safety and effectiveness of foam-filled structures.

A significant merit of this research is the comprehensive study of the tearing mechanism in PVC foams subjected to different loading and boundary conditions. We have revealed that bending actions increase in-plane tearing while decreasing through-the-thickness tearing. For instance, the tearing strength in the *x*-direction (in-plane tearing) decreases by around 17% when the PVC foam moves downward by 3 mm



Fig. 15 Damage contour plots in the PVC foam at $\Delta_z = 60$ mm using the 3D-PDM: a unconfined in the *x*-direction case; **b** confined in the *x*-direction case



(3.75% of its height) under the bending actions, while the tearing strength in the *z*-direction (through-the-thickness tearing) increases by around 11%. Additionally, confining the PVC foam in the x-direction accelerates the tearing in the z-direction. This new understanding of tearing fracture behavior with respect to certain mechanical conditions broadens the comprehension of the mechanics of PVC foams.

The results presented in this work open up possibilities for implementing peridynamic simulations in a broader range of polymeric and composite materials. The success of the peridynamic approach in fracture mechanics proves its ability to be used on a wide range in the foreseeable future. Nevertheless, this study enhances the comprehension of PVC foam fracture behavior and offers a strong foundation for new research regarding fracture mechanics in advanced materials done in peridynamic simulations.

Funding Open access funding provided by The Hong Kong Polytechnic University.

Data availability No data was used for the research described in the article.

Declarations

Conflict of interest The author declares that there are no conflict of interest.

Open Access This article is licensed under a Creative Commons Attribution 4.0 International License, which permits use, sharing, adaptation, distribution and reproduction in any medium or format, as long as you give appropriate credit to the original author(s) and the source, provide a link to the Creative Commons licence, and indicate if changes were made. The images or other third party material in this article are included in the article's Creative Commons licence, unless indicated otherwise in a credit line to the material. If material is not included in the article's Creative Commons licence and your intended use is not permitted by statutory regulation or exceeds the permitted use, you will need to obtain permission directly from the copyright holder. To view a copy of this licence, visit http://creativecommons.org/licenses/by/4.0/.

References

- Ahmadi E, Atrian A, Fesharaki JJ, Montazerolghaem H, Saberi S (2021) Experimental and numerical assessment of high-velocity impact behavior of syntactic foam core sandwich structures. Eur J Mech A/Solids 90:104355. https://doi.org/10.1016/j.euromechsol. 2021.104355
- Crépin D (2022) Toward toughness improvement of foam core sandwich panel inserts through an energy approach. Eur J Mech A/Solids 94:104575. https://doi.org/10.1016/j.euromechsol.2022. 104575
- Li H, Ying Wu, Lingyan Wu, Cui C, Niu K (2024) Innovative CF/PVC foam applicated for automotive synthetic leather with high-performance and reduced VOC emissions. Materials 17(5):1076. https://doi.org/10.3390/ma17051076
- Chen Y, Das R (2022) A review on manufacture of polymeric foam cores for sandwich structures of complex shape in automotive applications. J Sandw Struct Mater 24(1):789–819. https://doi.org/ 10.1177/10996362211030564
- Zhou T, Zhang P, Xiao W, Liu J, Cheng Y (2019) Experimental investigation on the performance of PVC foam core sandwich panels under air blast loading. Compos Struct 226:111081. https://doi. org/10.1016/j.compstruct.2019.111081
- Chen Q, Linghu T, Gao Y, Wang Z, Liu Y, Du R, Zhao G (2017) Mechanical properties in glass fiber PVC-foam sandwich structures from different chopped fiber interfacial reinforcement through vacuum-assisted resin transfer molding (VARTM) processing. Compos Sci Technol 144:202–207. https://doi.org/10.1016/j.compscitech.2017.03.033
- Bolf D, Zamarin A, Krolo P, Hadjina M (2022) Experimental evaluation of shear properties of lightweight PVC core for marine application using digital image correlation system. J Mar Sci Eng 10(2):280. https://doi.org/10.3390/jmse10020280
- Robin A, Davies P, Arhant M, Le Jeune S, Lacotte N, Morineau E, Ioos F, Dourlen P, Cairo R (2024) Mechanical performance of sandwich materials with reduced environmental impact for marine structures. J Sandw Struct Mater 26:99–113. https://doi.org/10. 1177/10996362221127975
- Sadler RL, Sharpe M, Panduranga R, Shivakumar K (2009) Water immersion effect on swelling and compression properties of ecocore, PVC foam and balsa wood. Compos Struct 90:330–336. https://doi.org/10.1016/j.compstruct.2009.03.016
- Aliha MRM, Mousavi SS, Bahmani A, Linul E, Marsavina L (2019) Crack initiation angles and propagation paths in polyurethane foams under mixed modes I/II and I/III loading. Theor Appl Fract Mech 101:152–161. https://doi.org/10.1016/j.tafmec.2019.02.016
- Imani DM, Aliha MRM, Linul E, Marsavina L (2022) A suitable mixed mode I/II test specimen for fracture toughness study of



- polyurethane foam with different cell densities. Theor Appl Fract Mech 117:103171. https://doi.org/10.1016/j.tafmec.2021.103171
- Chen S, Isaksson P (2018) An experimental analysis of the defect sensitivity of solid foams. Theor Appl Fract Mech 96:768–774. https://doi.org/10.1016/j.tafmec.2017.11.004
- Tang Y, Li Y, Jiang X, Zhao J, Zhao G, Xie W, Zhang W (2024) Tensile properties of transversely isotropic closed-cell PVC foam under quasi-static and dynamic loadings. J Sandw Struct Mater 26:373–395. https://doi.org/10.1177/10996362231209013
- Liu Y, Rahimidehgolan F, Altenhof W (2020) Anisotropic compressive behavior of rigid PVC foam at strain rates up to 200 s⁻¹. Polymer Test 91:106836. https://doi.org/10.1016/j.polymertesting. 2020.106836s
- Mharsi K, Fajoui J, Casari P, Kchaou M (2023) Experimental study of the mechanical behavior of polyvinyl chloride foam under shear stress. J Mater Eng Perform 32:7879–7894. https://doi.org/ 10.1007/s11665-022-07672-w
- Mostafa A, Shankar K, Morozov EV (2014) Experimental, theoretical and numerical investigation of the flexural behaviour of the composite sandwich panels with PVC foam core. Appl Compos Mater 21:661–675. https://doi.org/10.1007/s10443-013-9361-4
- Dai K, Jiang T, Zhao M, Yuxin Xu, Zhao X, Bian J (2024) Numerical analysis on the dynamic response of PVC foam/polyurea composite sandwich panels under the close air blast loading. Polymers 16(6):810. https://doi.org/10.3390/polym16060810
- Yang L, Li X, Zi F, Yang S, Zhang Z, Qu J, Dong Y, Wu L (2022) Dynamic response of graded PVC foam sandwich panel under air blast loads. Mech Adv Mater Struct 29:3694–3708. https://doi.org/ 10.1080/15376494.2021.1909190
- Zhou T, Cheng Y, Zhao Y, Zhang L, Wang H, Chen G, Liu J, Zhang P (2020) Experimental investigation on the performance of PVC foam core sandwich panels subjected to contact underwater explosion. Compos Struct 235:111796. https://doi.org/10.1016/j. compstruct.2019.111796
- Şerban DA, Linul E (2023) Fatigue behaviour of closed-cell polyurethane rigid foams. Eng Fail Anal 154:107728. https://doi. org/10.1016/j.engfailanal.2023.107728
- Wei Y (2006) A new finite element method for strain gradient theories and applications to fracture analyses. Eur J Mech A/Solids 25:897–913. https://doi.org/10.1016/j.euromechsol.2006.03.001
- Funari MF, Spadea S, Lonetti P, Lourenço PB (2021) On the elastic and mixed-mode fracture properties of PVC foam. Theor Appl Fract Mech 112:102924. https://doi.org/10.1016/j.tafmec.2021.10 2924
- Santos JPJR, Correia DS, Marques EAS, Carbas RJC, Gilbert F, da Silva LFM (2023) Extended finite element method (XFEM) model for the damage mechanisms present in joints bonded using adhesives doped with inorganic fillers. Materials 16(23):7499. https:// doi.org/10.3390/ma16237499
- Marsavina L, Constantinescu DM, Linul E, Stuparu FA, Apostol DA (2016) Experimental and numerical crack paths in PUR foams. Eng Fract Mech 167:68–83. https://doi.org/10.1016/j.engfracmech.2016.03.043
- Ebadi-Rajoli J, Akhavan-Safar A, Hosseini-Toudeshky H, da Silva LFM (2020) Progressive damage modeling of composite materials subjected to mixed mode cyclic loading using cohesive zone model. Mech Mater 143:103322. https://doi.org/10.1016/j.mechmat.2020. 103322
- Liu CW, Chiu TC (2023) Cohesive-zone based fracture mechanics model of an edge delamination in bimaterial beam under mixedmode bending test. Eur J Mech A/Solids 99:104928. https://doi. org/10.1016/j.euromechsol.2023.104928
- Wang M, Gao K, Feng YT (2021) An improved continuum-based finite—discrete element method with intra-element fracturing algorithm. Comput Methods Appl Mech Eng 384:113978. https://doi. org/10.1016/j.cma.2021.113978

- Yang ZJ, Chen J (2005) Finite element modelling of multiple cohesive discrete crack propagation in reinforced concrete beams. Eng Fract Mech 72:2280–2297. https://doi.org/10.1016/j.engfracmech. 2005 02 004
- Wawrzynek PA, Ingraffea AR (1989) An interactive approach to local remeshing around a propagating crack. Finite Elem Anal Des 5(1):87–96. https://doi.org/10.1016/0168-874X(89)90008-5
- Shahani AR, Amini Fasakhodi MR (2009) Finite element analysis of dynamic crack propagation using remeshing technique. Mater Des 30:1032–1041. https://doi.org/10.1016/j.matdes.2008.06.049
- Silling SA (2000) Reformulation of elasticity theory for discontinuities and long-range forces. J Mech Phys Solids 48:175–209. https://doi.org/10.1016/S0022-5096(99)00029-0
- 32. Silling SA, Askari E (2005) A meshfree method based on the peridynamic model of solid mechanics. Comput Struct 83:1526–1535. https://doi.org/10.1016/j.compstruc.2004.11.026
- Abdoh DA (2024) Three-dimensional modeling of impact fractures in brittle materials via peridynamics. Eng Fract Mech 297:109884. https://doi.org/10.1016/j.engfracmech.2024.109884
- 34. Zhang L, Ouyang D, Mao R, Qin X, Liu Q, Xie Q (2024) A study on the damage characteristics of glass under the combined effects of explosion and high temperature: an analysis using peridynamics. Eng Fail Anal 159:108084. https://doi.org/10.1016/j.engfailanal. 2024.108084
- Abdoh DA (2024) Three-dimensional peridynamic modeling of deformations and fractures in steel beam-column welded connections. Eng Fail Anal 160:108155. https://doi.org/10.1016/j.engfai lanal.2024.108155
- Dong W, Li S, Wang X, He Q, Wang P, An B, Yang B, Ding J, Huang J (2024) Study on fatigue damage tolerance of rail steel materials using peridynamics. Eng Fail Anal 159:108138. https:// doi.org/10.1016/j.engfailanal.2024.108138
- Abdoh DA (2024) Failure analysis of bolted steel plate connections with three-dimensional flexibilities. Int J Mech Sci 272:109313. https://doi.org/10.1016/j.ijmecsci.2024.109313
- Abdoh DA (2024) A novel and efficient computational peridynamic framework for modeling explosive blast effects on solid plates. Comput Struct 299:107381. https://doi.org/10.1016/j.comp struc.2024.107381
- 39. Sheikhbahaei P, Mossaiby F, Shojaei A (2023) Analyzing cyclic loading behavior of concrete structures: a peridynamic approach with softening models and validation. Theor Appl Fract Mech 128:104165. https://doi.org/10.1016/j.tafmec.2023.104165
- Sau N, Medina-Mendoza J, Borbon-Almada AC (2019) Peridynamic modelling of reinforced concrete structures. Eng Fail Anal 103:266–274. https://doi.org/10.1016/j.engfailanal.2019.05.004
- Zhang X, Ding J, Zhang Y (2023) A rate-dependent peridynamic model of reinforced concrete subjected to explosive loading. Eng Fract Mech 292:109666. https://doi.org/10.1016/j.engfracm ech.2023.109666
- Abdoh DA, Yin BB, Kodur VKR, Liew KM (2022) Computationally efficient and effective peridynamic model for cracks and fractures in homogeneous and heterogeneous materials. Comput Methods Appl Mech Eng 399:115318. https://doi.org/10.1016/j.cma.2022.115318
- Zhiyong Chen J, Woody Ju, Guoshao Su, Huang X, Li S, Zhai L (2019) Influence of micro-modulus functions on peridynamics simulation of crack propagation and branching in brittle materials. Eng Fract Mech 216:106498. https://doi.org/10.1016/j.engfracmech.2019.106498
- Yang Y, Chen Y, Liu Y (2024) Fracture analysis of hyperelastic membrane using bond-associated non-ordinary state-based peridynamics. Eng Fract Mech 303:110131. https://doi.org/10.1016/j. engfracmech.2024.110131
- Li C, Zhang H, Ye H, Zhang H, Zheng Y (2023) An improved stabilized peridynamic correspondence material model for the crack



propagation of nearly incompressible hyperelastic materials. Comput Methods Appl Mech Eng 404:115840. https://doi.org/10.1016/j.cma.2022.115840

Publisher's Note Springer Nature remains neutral with regard to jurisdictional claims in published maps and institutional affiliations.

